

# Climate Dynamics

## The Modulation of the Southern Africa Precipitation Response to the El Niño Southern Oscillation by the Subtropical Indian Ocean Dipole --Manuscript Draft--

|  |  |
|--|--|
| <b>Manuscript Number:</b>                            | CLDY-D-15-00736  |
| <b>Full Title:</b>                                   | The Modulation of the Southern Africa Precipitation Response to the El Niño Southern Oscillation by the Subtropical Indian Ocean Dipole  |
| <b>Article Type:</b>                                 | Original Article   |
| <b>Keywords:</b>                                     | Southern Africa; Precipitation; El Nino-Southern Oscillation; Subtropical Indian Ocean Dipole  |
| <b>Corresponding Author:</b>                         | Andrew Hoell<br>UNITED STATES  |
| <b>Corresponding Author Secondary Information:</b>   |  |
| <b>Corresponding Author's Institution:</b>           |  |
| <b>Corresponding Author's Secondary Institution:</b> |  |
| <b>First Author:</b>                                 | Andrew Hoell   |
| <b>First Author Secondary Information:</b>           |  |
| <b>Order of Authors:</b>                             | Andrew Hoell<br>Chris Funk<br>Jens Zinke<br>Laura Harrison   |
| <b>Order of Authors Secondary Information:</b>       |  |
| <b>Funding Information:</b>                          |  |
| <b>Abstract:</b>                                     | <p>The climate of Southern Africa, defined as the land area bound by the region 15°S-35°S; 12.5°E-42.5°E, during the November-March rainy season is driven by Indo-Pacific sea surface temperature (SST) anomaly expressions associated with the El Niño Southern Oscillation (ENSO) and the Subtropical Indian Ocean Dipole (SIOD). The observed November-April 1979-2014 Southern Africa precipitation during the four ENSO and SIOD phase combinations suggests that the phase of the SIOD can disrupt or enhance the Southern Africa precipitation response during ENSO. Here, we use a large ensemble of model simulations driven by global SST and ENSO-only SST to test whether the SIOD modifies the relationship between Southern Africa precipitation and ENSO. Since ENSO-based precipitation forecasts are used extensively over Southern Africa, an improved understanding of how other modes of SST variability modulate the regional response to ENSO is important.</p> <p>ENSO, in the absence of the SIOD, forces an equivalent barotropic Rossby wave over Southern Africa that modifies the regional mid-tropospheric vertical motions and precipitation. El Niño (La Niña) is related with high (low) pressure over Southern Africa that produces anomalous mid-tropospheric descent (ascent) and decreases (increases) in precipitation relative to average. When the SIOD and ENSO are in opposite phases, the SIOD complements the ENSO-related atmospheric response over Southern Africa by strengthening the regional equivalent barotropic Rossby wave, anomalous mid-tropospheric vertical motions and anomalous precipitation. In contrast, when the SIOD and ENSO are in the same phase, the SIOD disrupts the ENSO-related atmospheric response over Southern Africa by weakening the regional equivalent barotropic Rossby wave, anomalous mid-tropospheric vertical motions and anomalous precipitation.</p> |

|                             |  |
|-----------------------------|--|
| <b>Suggested Reviewers:</b> | Swadhin Behera<br>behera@jamsetc.go.jp |
|                             | J.V. Ratnam<br>jvratnam@jamsetc.go.jp  |
|                             | Chris Reason<br>chris.reason@uct.ac.za |
|                             | D. Manatsa<br>dmanatsa@gmail.com       |

[Click here to view linked References](#)

1     **The Modulation of the Southern Africa Precipitation Response to the El Niño**

2                   **Southern Oscillation by the Subtropical Indian Ocean Dipole**

3

4                                   Andrew Hoell<sup>1</sup>

5                   *NOAA Earth System Research Laboratory Physical Sciences Division*

6

7                                   Chris Funk

8                   *Department of Geography University of California Santa Barbara*

9                                   *U.S. Geological Survey*

10

11                                   Jens Zinke

12                   *Department of Environment and Agriculture, Curtin University of Technology*

13                   *School of Geography, Archaeology and Environmental Studies, University of*

14                                   *Witwatersrand*

15

---

<sup>1</sup> Corresponding Author Address: Andrew Hoell, NOAA/ESRL/PSD, 325  
Broadway, Boulder, CO 80305, email: [andrew.hoell@noaa.gov](mailto:andrew.hoell@noaa.gov)

16

Laura Harrison

17

*Department of Geography University of California Santa Barbara*

18

19

20

21

22

3 December 2015

23

24

## Abstract

25           The climate of Southern Africa, defined as the land area bound by the region  
26 15°S-35°S; 12.5°E-42.5°E, during the November-March rainy season is driven by Indo-  
27 Pacific sea surface temperature (SST) anomaly expressions associated with the El  
28 Niño Southern Oscillation (ENSO) and the Subtropical Indian Ocean Dipole (SIOD).  
29 The observed November-April 1979-2014 Southern Africa precipitation during the  
30 four ENSO and SIOD phase combinations suggests that the phase of the SIOD can  
31 disrupt or enhance the Southern Africa precipitation response during ENSO. Here,  
32 we use a large ensemble of model simulations driven by global SST and ENSO-only  
33 SST to test whether the SIOD modifies the relationship between Southern Africa  
34 precipitation and ENSO. Since ENSO-based precipitation forecasts are used  
35 extensively over Southern Africa, an improved understanding of how other modes of  
36 SST variability modulate the regional response to ENSO is important.

37           ENSO, in the absence of the SIOD, forces an equivalent barotropic Rossby  
38 wave over Southern Africa that modifies the regional mid-tropospheric vertical  
39 motions and precipitation. El Niño (La Niña) is related with high (low) pressure over  
40 Southern Africa that produces anomalous mid-tropospheric descent (ascent) and

41 decreases (increases) in precipitation relative to average. When the SIOD and ENSO  
42 are in opposite phases, the SIOD compliments the ENSO-related atmospheric  
43 response over Southern Africa by strengthening the regional equivalent barotropic  
44 Rossby wave, anomalous mid-tropospheric vertical motions and anomalous  
45 precipitation. In contrast, when the SIOD and ENSO are in the same phase, the SIOD  
46 disrupts the ENSO-related atmospheric response over Southern Africa by weakening  
47 the regional equivalent barotropic Rossby wave, anomalous mid-tropospheric vertical  
48 motions and anomalous precipitation.

## 49 **1. Introduction**

50 The climate of Southern Africa, defined as the land area bound by the region  
51 15°S-35°S; 12.5°E-42.5°E, is related with the simultaneous spatial variations of Pacific,  
52 Indian and Atlantic Ocean sea surface temperatures (SST) (e.g. Nicholson and Kim  
53 1997). The Indo-Pacific Ocean SST anomaly expressions related to Southern Africa  
54 climate have been shown to be a consequence of three modes of SST variability: the  
55 El Niño Southern Oscillation (ENSO) shown in Fig. 1a, the Indian Ocean Dipole (IOD)  
56 (e.g., Chambers et al, 1999; Webster et al, 1999; Saji et al, 1999) shown in Fig. 1b and  
57 the Subtropical Indian Ocean Dipole (SIOD) (Behera et al. 2000, Behera and  
58 Yamagata 2001) shown in Fig. 1c. In this manuscript, we examine how modes of  
59 Indo-Pacific SST variability simultaneously force Southern Africa precipitation during  
60 the November-March rainy season.

61 In aggregate, ENSO events force atmospheric circulations over Southern Africa  
62 that result in regional precipitation anomalies (e.g. Nicholson and Entekhabi 1986,  
63 Lindesay 1988, Jury et al. 1994, Rocha and Simmonds 1997, Nicholson and Kim 1997,  
64 Reason et al 2000, Misra 2003). A mid-tropospheric convection dipole between the  
65 region that includes the eastern Indian Ocean and Maritime Continent and the

66 central Pacific Ocean during ENSO events excites Rossby waves over Southern Africa  
67 (Ratnam et al. 2014, Hoell et al. 2015) that modifies the regional moisture fluxes  
68 (Reason and Jagadheesha 2005, Hoell et al. 2015) and vertical motions (Hoell et al.  
69 2015) thereby forcing the regional precipitation (Nicholson and Kim 1997). El Niño  
70 (La Niña), forces high (low) pressure over Southern Africa, which in turn forces  
71 anomalous reductions (increases) in moisture fluxes, anomalous downward (upward)  
72 vertical motions and decreases (increases) in precipitation relative to average.

73         There is considerable inter-event variability in the Atlantic and Indo-Pacific  
74 SST (Wrytki 1975) and the atmospheric teleconnections driven by those SST over  
75 Southern Africa between each El Niño and La Niña (Ratnam et al. 2014, Hoell et al.  
76 2015). El Niño and La Niña-forced atmospheric teleconnections over Southern Africa  
77 during November-March are modified by SST variability over the Atlantic and Indian  
78 Oceans (Nicholson 1997, Goddard and Graham 1999). Observational analyses have  
79 suggested that atmospheric teleconnections during La Niña are more sensitive to SST  
80 forcing over the Atlantic Ocean while atmospheric teleconnections during El Niño are  
81 more sensitive to SST forcing over the Indian Ocean (Nicholson and Kim 1997).  
82 Problematically, the differences in the SST expressions between seemingly similar El



83 Niño and La Niña events can compromise the potential predictability of Southern  
84 Africa precipitation. Therefore, we reexamine the critical role that Indian Ocean SSTs  
85 play in modifying the ENSO-driven Southern Africa precipitation during the  
86 November-March rainy season.

87 Indian Ocean SST variability on seasonal to interannual time scales is largely  
88 expressed in the form of dipole patterns across the ocean basin as a result of the  
89 SIOD (Behera et al. 2000, Behera and Yamagata 2001) whose SST expression is shown  
90 in Fig. 1c and the IOD (e.g., Chambers et al, 1999; Webster et al, 1999; Saji et al,  
91 1999) whose SST expression is shown in Fig. 1b. The SST anomaly expression of the  
92 SIOD (Fig. 2c) forces atmospheric circulations over Southern Africa that modifies the  
93 flux of moisture and therefore precipitation (Reason 2001, Washington and Preston  
94 2006). The SST anomaly expression of the IOD (Fig. 1b) forces wide-ranging  
95 teleconnections across the Indian Ocean basin and surrounding areas by modifying  
96 the zonal winds (Saji et al. 1999) and therefore moisture fluxes over Africa (Behera et  
97 al. 2005).

98 The relative effects of Indian Ocean SST and Pacific Ocean SST on Southern  
99 Africa climate are currently unknown. Manatsa (2011a, 2011b) attempted to

100 decouple the effect of the IOD and ENSO on the leading components of Southern  
101 Africa rainfall using observational data. Manatsa (2011a, 2011b) had limited success  
102 due to what appeared to be changes in the behavior of the atmospheric circulation  
103 during the 1970s and 1990s. However, what is known is that atmospheric models  
104 forced by Indian Ocean and Pacific Ocean SST more accurately depict the climate of  
105 Southern Africa as compared to the forcing by Pacific SST alone (Reason and  
106 Jagadheesha 2005). Therefore, understanding the simultaneous effects of Indo-  
107 Pacific SST on Southern African climate is important.

108         The global SST anomaly pattern related to the observed November-March  
109 1979-2014 Southern Africa precipitation variability is shown in Fig. 2b. Observed  
110 Southern Africa precipitation (Fig. 2b) is related with ENSO (Fig. 1a) and a southwest  
111 to northeast oriented dipole SST pattern in the Indian Ocean that is similar to the  
112 SST anomaly expression of the SIOD (Fig. 1c). The SST anomaly expression of the  
113 IOD (Fig. 1b) is unrelated with historical Southern Africa precipitation during  
114 November-March (Fig. 2b). Enhanced Southern Africa precipitation is related with La  
115 Niña, defined by a cool east-central tropical Pacific Ocean, and a positive SIOD,  
116 defined by a warm southwest Indian Ocean and cool central Indian Ocean. Reduced

117 Southern Africa precipitation is related with El Niño, defined by a warm east-central  
118 tropical Pacific Ocean, and a negative SIOD, defined by a cool southwest Indian  
119 Ocean and a warm central Indian Ocean. Overall, the observed Southern Africa  
120 precipitation (Fig. 2b) is most closely related to opposing phases of ENSO and the  
121 SIOD.

122         Observed conditions during 1979-2014 indicate that differences in the  
123 simultaneous phasing of ENSO and the SIOD results in precipitation anomalies of  
124 varying strength over Southern Africa during November-March (Fig. 3). When ENSO  
125 and the SIOD were out of phase, Southern Africa precipitation was strongly reduced  
126 during El Niño (Fig. 3a-b) and Southern Africa precipitation was strongly enhanced  
127 during La Niña (Fig. 3e-f). In contrast, when ENSO and the SIOD were in phase,  
128 Southern Africa precipitation was only marginally reduced during El Niño (Fig. 3c-d)  
129 and Southern Africa precipitation was only marginally enhanced during La Niña (Fig.  
130 3g-h). The observed November-April 1979-2014 Southern Africa precipitation during  
131 the four ENSO and SIOD phase combinations suggests that the phase of the SIOD  
132 can disrupt or enhance the Southern Africa precipitation response during ENSO.

133           In this manuscript, we examine how the phase of the SIOD, and therefore the  
134 SST anomaly expression of the Indian Ocean, modulates the Southern Africa  
135 precipitation response to ENSO through comparisons of two large atmospheric  
136 simulation ensembles for 1979-2014. The first ensemble is forced by global SST  
137 variability, which includes the combined effects of ENSO and the SIOD, and the  
138 second ensemble is forced by SST variability associated only with ENSO. We test the  
139 degree to which the SIOD modulates the ENSO-related precipitation response over  
140 Southern Africa by comparing the historical atmospheric simulation ensembles  
141 separated by phase of the SIOD. In section 2, we describe the observed historical  
142 data and the two atmospheric simulations ensembles utilized. In section 3, we  
143 examine how the SIOD modulates the atmospheric teleconnections and precipitation  
144 associated with ENSO over Southern Africa. In section 4, we provide a summary.

145

## 146 **2. Data, Models and Methods**

### 147 *2.1 Observed Data*

148           Observed historical precipitation for 1979-2014 is from the Global  
149 Precipitation Climatology Project (GPCP) blended satellite and rain gauge estimates

150 version 2.2 on a 2.5°x2.5° latitude-longitude fixed grid (Adler et al. 2003, Huffman et  
151 al. 2009). Observed historical SSTs for 1979-2014 are from the merged Hadley-  
152 NOAA Optimum Interpolation dataset developed by Hurrell et al. (2008) on a  
153 1.0°x1.0° latitude-longitude fixed grid. Observed SST and sea ice from Hurrell et al.  
154 (2008) also specify the ocean boundary conditions in historical atmospheric model  
155 simulations, commonly referred to as AMIP simulations after the Atmospheric Model  
156 Intercomparison Project (Gates 1992).

157

## 158 *2.2 AMIP Simulations*

159 Two separate AMIP experiments for 1979-2014 are used to test whether the  
160 SIOD modulates the Southern Africa precipitation response to ENSO during the  
161 November-March rainy season. The two AMIP experiments are each made up of 80  
162 ensembles, 30 of which are generated using the ECHAM5 model (Roeckner et al.  
163 2006) and 50 of which are generated using the GFS version 2 model (Saha et al.  
164 2010).

165 The first AMIP experiment is used to test the atmospheric response to the  
166 observed global SST, and is driven by time-varying historical monthly global SST, sea

167 ice, greenhouse gas concentrations and aerosols for 1979-2014. The second AMIP  
168 experiment is used to test the atmospheric response to ENSO, and is driven by the  
169 leading pattern of global time-varying monthly SST anomaly added to the monthly  
170 climatology, observed sea ice, greenhouse gas concentrations and aerosols for 1979-  
171 2014.

172         The leading pattern of global SST anomaly used to specify the ocean  
173 boundary condition in the second AMIP experiment was identified by a covariance-  
174 based empirical orthogonal function (EOF) calculation of detrended monthly SST  
175 from January 1978-December 2011 (Fig. 4). The leading pattern of SST and the AMIP  
176 experiment driven by the leading pattern of SST are hereafter referred to as EOF1.  
177 The spatial pattern of EOF1 (Fig. 4a) closely resembles the SST anomaly expression of  
178 ENSO (Fig. 1a), and the principal component of EOF1 (Fig. 4b) is correlated with the  
179 Niño3.4 index at  $r=0.97$ . For 2012-2014, the principal component of EOF1 is  
180 calculated by projecting the EOF pattern (Fig. 3a) on to SSTs. The monthly SST  
181 expression related to EOF1 for 1979-2014 is obtained by multiplying EOF1 (Fig. 4a)  
182 by its principal component (Fig. 4b). The monthly SST anomaly of EOF1 is added to  
183 the 1979-2010 monthly SST climatology to obtain the time-varying monthly SST used

184 as the ocean boundary condition of the AMIP simulations. For more information on  
185 these experiments please visit the URL  
186 <http://www.esrl.noaa.gov/psd/repository/alias/facts>.

187

### 188 *2.3 Comparison of Observed and Simulated Southern Africa Precipitation*

189 The monthly average 1979-2014 observed precipitation over Southern Africa  
190 indicates that the primary precipitation season spans November-March (Fig. 5b).  
191 November-March 1979-2014 observed average precipitation over Southern Africa is  
192 unevenly distributed in space (Fig. 5a). Regionally, the greatest precipitation  
193 amounts during November-March fall over Malawi, Angola, Zambia and Mozambique  
194 while the lowest precipitation amounts fall over the Atlantic facing coastlines of  
195 southwest Southern Africa (Fig. 5a).

196 The monthly averaged precipitation variability of the ECHAM5 and GFS  
197 version 2 AMIP simulations driven by observed global time-varying SST (Fig. 5d,f) are  
198 very similar to the observed precipitation (Fig. 3b), with correlations in excess of 0.98.  
199 While the correlation between the observed monthly precipitation climatology and  
200 the climatology of the AMIP simulations driven by global SST over Southern Africa

201 are very similar, there is a dry bias in the ECHAM5 and GFS version 2 models of  
202 about 30% each month. Due to this dry bias we show standardized precipitation  
203 anomalies in time and space in the following analyses. Standardized precipitation  
204 anomalies are defined as the precipitation anomaly divided by the seasonal cycle  
205 standard deviation of precipitation. The average November-March 1979-2014  
206 precipitation of the ECHAM5 and GFS version 2 AMIP simulations driven by observed  
207 global time-varying SST over Southern Africa (Figs. 5c,e) are similar in space to the  
208 observed precipitation (Fig. 5a).

209         The temporal variability of observed precipitation and precipitation resolved  
210 by AMIP simulations driven by global SST and EOF1 of SST over Southern Africa for  
211 November-March 1979-2014 are shown in Figs. 6a and 6b, respectively. The  
212 ensemble average precipitation variability of the AMIP simulations driven by global  
213 SST and EOF1 of SST during November-March 1979-2014 capture in excess of 25%  
214 of the variance of observed precipitation over Southern Africa (Fig. 6a). The AMIP  
215 experiments capture the interannual variability and magnitude of standardized  
216 precipitation anomalies well during prolonged periods. Furthermore, the observed  
217 precipitation always falls within the 80-member ensemble spread of the AMIP



218 simulations. The results presented here show that the AMIP simulations forced by  
219 global SST and EOF1 of SST capture the precipitation climatology and variability of  
220 Southern Africa well and are suitable to test the SST effects on Southern Africa.

221

### 222 **3. Southern Africa Precipitation Sensitivity to ENSO**

223 Fig. 7a shows the correlation of observed SST and Southern Africa  
224 precipitation variability in AMIP simulations driven by global SST for November-  
225 March 1979-2014. The AMIP simulations driven by global SST affirm the historical  
226 observed relationship between SST and Southern Africa precipitation (Fig. 2b).  
227 Southern Africa precipitation is associated with ENSO (Fig. 1a) and a southwest-to-  
228 northeast dipole of SST in the Indian Ocean similar to the SST anomaly expression of  
229 the SIOD (Fig. 1c). AMIP simulations driven by global SST (Fig. 6a) also affirm  
230 observed historical conditions in that the IOD (Fig. 1b) is not significantly related with  
231 November-March Southern Africa precipitation.

232 Fig. 7b shows the correlation of observed SST and Southern Africa  
233 precipitation in AMIP simulations driven by EOF1 of SST for November-March 1979-  
234 2014 to test the degree to which ENSO alone is related with Southern Africa

235 precipitation. The AMIP simulations driven by EOF1 once again affirm the observed  
236 historical relationship between ENSO and Southern Africa precipitation (Fig. 2b), with  
237 similar spatial correlations to the AMIP simulations driven by global SST over the  
238 central Pacific Ocean (Fig. 7a). The relationship between Indian Ocean SST and  
239 Southern Africa precipitation driven by EOF1 of SST are weak, as evidenced by weak,  
240 yet significant, correlations over the central Indian Ocean (Fig. 7b) that are present in  
241 EOF1 (Fig. 4a). The SST anomaly expression associated with Southern Africa  
242 precipitation in AMIP simulations driven by EOF1 (Fig. 7b) does not include the SST  
243 anomaly expression of the SIOD (Fig. 1c) in contrast with the AMIP simulations driven  
244 by global SST (Fig. 7a).

245         Since the SIOD is not fully realized in the forcing of Southern Africa  
246 precipitation by EOF1 (Fig. 7b), but is fully realized in the forcing of Southern Africa  
247 precipitation by global SST (Fig. 7a), we are able to test whether the SIOD modifies  
248 the relationship between Southern Africa precipitation and ENSO through a  
249 comparison of these two experimental suites. We test whether the SIOD modifies  
250 the relationship between Southern Africa precipitation and ENSO through an

251 examination of Southern Africa precipitation as a function of SIOD phase in AMIP  
252 simulations forced by global SST and EOF1 of SST.

253 Fig. 8 shows the relationship between Southern Africa precipitation, SST and  
254 ENSO separated by phase of the SIOD in AMIP simulations forced by global SST.  
255 When all November-March seasons are considered, Southern Africa precipitation is  
256 associated with the SST anomaly expressions (Fig. 8a) of ENSO (Fig. 1a) and the SIOD  
257 (Fig. 1c), and is significantly correlated with the Niño3.4 index (Fig. 8b). When the  
258 Niño3.4 and SIOD indices have the opposite sign during November-March, Southern  
259 Africa precipitation is again associated with the SST anomaly expressions (Fig. 8c) of  
260 ENSO (Fig. 1a) and the SIOD (Fig. 1c), and is significantly correlated with the Niño3.4  
261 index (Fig. 8d). The difference between the condition in which the Niño3.4 and SIOD  
262 indices have the opposite sign and when all seasons are considered is that the  
263 relationship between Southern Africa precipitation and Indo-Pacific SSTs is stronger  
264 when the Niño3.4 and SIOD indices have the opposite sign. When the Niño3.4 and  
265 SIOD indices have the same sign during November-March, Southern Africa  
266 precipitation is associated with an SST anomaly (Fig. 8e) that does not resemble  
267 either the ENSO (Fig. 1a) or the SIOD (Fig. 1c) SST anomaly expressions. In fact,

268 when the SIOD and ENSO are in the same phase, Southern Africa precipitation is  
269 only closely related with a coherent pattern of western Indian Ocean SST (Fig. 8e).

270 This examination of Southern Africa precipitation as a function of the SIOD  
271 phasing indicates that the SIOD modulates the Southern Africa precipitation response  
272 to ENSO. When the SIOD and Niño3.4 indices have the opposite sign, which results  
273 in an SST expression that closely resembles the historical SST and Southern Africa  
274 precipitation relationship (Fig. 2b), this condition results in a stronger Southern Africa  
275 precipitation response (Fig. 8). When the SIOD and Niño3.4 indices have the same  
276 sign, Southern Africa precipitation is not related to the SST anomaly expressions (Fig.  
277 8e) of ENSO (Fig. 1a) or the SIOD (Fig. 1c). Depending on the phase of the SIOD, the  
278 effect of the SIOD can either compliment the Southern Africa precipitation response  
279 to ENSO, or can disrupt the Southern Africa precipitation response to ENSO,  
280 affirming the small sample of observed conditions (Fig. 3).

281 The atmospheric circulation over Southern Africa associated with ENSO and  
282 separated by phase of the SIOD during November-March in AMIP simulations forced  
283 by global SSTs is shown in Fig. 9. When all November-March seasons are  
284 considered, ENSO is related to an equivalent barotropic Rossby wave over Southern

285 Africa, that modifies the regional mid-tropospheric vertical motions and precipitation.  
286 El Niño (La Niña) is related with high (low) pressure over Southern Africa (vectors in  
287 Fig. 9b) that is responsible for anomalous mid-tropospheric descent (ascent) (Fig. 9b)  
288 and decreases (increases) in precipitation relative to average (Fig. 9a). When the  
289 Niño3.4 and SIOD indices have the opposite sign during November-March, the SIOD  
290 compliments the ENSO-related atmospheric response over Southern Africa by  
291 strengthening the equivalent barotropic Rossby wave (Fig. 9d), anomalous mid-  
292 tropospheric vertical motions (Fig. 9d) and anomalous precipitation (Fig. 9d). When  
293 the Niño3.4 and SIOD indices have the same sign during November-March, the SIOD  
294 disrupts the ENSO-related atmospheric response over Southern Africa by weakening  
295 the equivalent barotropic Rossby wave (Fig. 9f) anomalous mid-tropospheric vertical  
296 motions (Fig. 9f) and anomalous precipitation (Fig. 9e).

297 Fig. 10 shows the relationship between Southern Africa precipitation, SST and  
298 ENSO separated by phase of the SIOD in AMIP simulations forced by EOF1 of SST.  
299 Note that the correlations of Southern Africa precipitation are to the full SST, and not  
300 EOF1 of SST, to demonstrate that the SIOD has no effect in the AMIP simulations  
301 driven by EOF1. When all November-March seasons are considered, Southern Africa

302 precipitation is associated with the SST anomaly expression (Fig. 10a) of EOF1 (Fig.  
303 4a), which by design is the same as the SST anomaly expression of ENSO (Fig. 1a).

304         When the Niño3.4 and SIOD indices have the opposite sign during  
305 November-March, Southern Africa precipitation in AMIP simulations forced by EOF1  
306 is related with the SST anomaly expression (Fig. 10c) of ENSO (Fig. 1a), as is  
307 expected. The SST anomaly expression of the SIOD also appears in this correlation,  
308 but only because the correlation is performed against the full SST field. The SIOD  
309 has no effect on Southern Africa precipitation in AMIP simulations driven by EOF1, as  
310 the relationship between Southern Africa precipitation and SST (Fig. 10c) is  
311 statistically indistinguishable from the aggregate case (Fig. 10a) over the tropical  
312 Pacific Ocean. This is in contrast with Southern Africa precipitation in AMIP  
313 simulations driven by global SST (Fig. 8), where the relationship between Southern  
314 Africa precipitation and ENSO significantly increased from the aggregate case when  
315 the SIOD and Niño3.4 indices are in the opposite phase (Fig. 8a,c).

316         When the Niño3.4 and SIOD indices have the same sign during November-  
317 March, Southern Africa precipitation in AMIP simulations forced by EOF1 is again  
318 related with the SST anomaly expression (Fig. 10d) of ENSO (Fig. 1a). The

319 southwestern dipole of the SST anomaly expression of the SIOD appears in this  
320 correlation only because the correlation is performed against the full SST field. The  
321 SIOD has no effect on Southern Africa precipitation in AMIP simulations forced by  
322 EOF1, as the relationship between Southern Africa precipitation (Fig. 10e) is  
323 statistically indistinguishable from the aggregate case (Fig. 10a) over the tropical  
324 Pacific Ocean.

325         The atmospheric circulations related to ENSO over Southern Africa in AMIP  
326 simulations forced by EOF1 are also statistically indistinguishable when separated by  
327 phase of the SIOD during November-March (Fig. 11). As was discussed previously,  
328 ENSO is related to an equivalent barotropic Rossby wave over Southern Africa, that  
329 modifies the regional mid-tropospheric vertical motions and precipitation (Fig. 11).

330

#### 331 **4. Summary and Discussion**

332         The historical ENSO and Southern Africa relationship (e.g. Fig. 2) has  
333 facilitated the successful prediction of Southern Africa precipitation during many  
334 November-March rainy seasons (e.g. Hastenrath et al. 1995). On average, La Niña is  
335 related with enhanced Southern Africa precipitation while El Niño is related with

336 reduced Southern Africa precipitation. However, there have been historical  
337 occurrences, namely 1983-1984, 1984-1985, 1985-1986, 1988-1989, 1995-1996, 1999-  
338 2000 and 2011-2012, in which La Niña events (Fig. 3g) occurred simultaneously with  
339 widespread areas of near average November-March precipitation over Southern  
340 Africa (Fig. 3h). Since the SIOD, a mode of SST variability in the Indian Ocean, is also  
341 related with Southern Africa precipitation, we examine whether the SIOD modulates  
342 the ENSO-related teleconnection over Southern Africa.

343       Observed historical relationships (Fig. 2) and AMIP simulations (Fig. 7) driven  
344 by global SST for November-March 1979-2014 indicate that Southern Africa  
345 precipitation is associated with ENSO (Fig. 1a) and the SIOD (Fig. 1c). Observed  
346 historical relationships (Fig. 2) and AMIP simulations (Fig. 7) driven by global SST also  
347 indicate that Southern Africa precipitation during November-March is unrelated with  
348 the IOD (Fig. 1b). Enhanced Southern Africa precipitation is related to La Niña,  
349 defined by a cool east-central tropical Pacific Ocean, and a positive SIOD, defined by  
350 a warm southwest Indian Ocean and cool central Indian Ocean. Reduced Southern  
351 Africa precipitation is related to El Niño, defined by a warm east-central tropical  
352 Pacific Ocean, and a negative SIOD, defined by a cool southwest Indian Ocean and a



353 warm central Indian Ocean. Overall, AMIP simulations driven by global SST and  
354 observed conditions indicate that Southern Africa precipitation is related to opposing  
355 phases of ENSO and the SIOD.

356         The average November-March 1979-2014 precipitation anomaly over  
357 Southern Africa during ENSO events in which ENSO and the SIOD were out of phase  
358 was much greater than the precipitation anomaly during ENSO events in which ENSO  
359 and SIOD were in phase (Fig. 3). Therefore, we examine whether the phase of the  
360 SIOD can modulate the relationship between ENSO and Southern Africa precipitation.

361         The modulation of the ENSO teleconnection over Southern Africa by the SIOD  
362 is tested through comparisons of two large atmospheric simulation ensembles for  
363 1979-2014. The first ensemble is forced by global SST variability, which includes the  
364 combined effects of ENSO and the SIOD, and the second ensemble is forced by SST  
365 variability associated only with ENSO. We test the degree to which the SIOD  
366 modulates the ENSO-related precipitation response over Southern Africa by  
367 comparing the two large historical atmospheric simulation ensembles separated by  
368 phase of the SIOD.

369 AMIP simulations driven by only ENSO indicate that ENSO forces an  
370 equivalent barotropic Rossby wave over Southern Africa that modifies the regional  
371 mid-tropospheric vertical motions and precipitation (Fig. 11). El Niño (La Niña) is  
372 related with high (low) pressure over Southern Africa that is responsible for  
373 anomalous mid-tropospheric descent (ascent) and decreases (increases) in  
374 precipitation relative to average.

375 The model simulations affirm observed conditions (Fig. 3) in that the SIOD can  
376 compliment or disrupt the Southern Africa precipitation response to ENSO (Figs. 8  
377 and 9). AMIP simulations driven by global SST indicate that opposing ENSO and  
378 SIOD phases generate complimentary telconnections that result in enhanced  
379 precipitation changes over Southern Africa. On the contrary, AMIP simulations driven  
380 by global SST indicate that when ENSO and the SIOD are in phase, the SIOD disrupts  
381 the ENSO-related teleconnections over Southern Africa by weakening the equivalent  
382 barotropic Rossby wave (Fig. 9f) anomalous mid-tropospheric vertical motions (Fig.  
383 9f) and anomalous precipitation (Fig. 9e).

384 Early methods of rainy season Southern Africa precipitation prediction were  
385 based only upon the statistical analyses of historical climate information (e.g.

386 Hastenrath et al. 1995). For the early statistical models, the predictors of Southern  
387 Africa precipitation included metrics of ENSO, expressed in terms SST or atmosphere-  
388 only indices such as the Southern Oscillation Index (SOI), and the atmospheric  
389 circulation. Southern Africa precipitation forecasts have evolved to include both  
390 statistical models and dynamical model forecasts simultaneously (Landman and  
391 Goddard 2005) or only dynamical model forecasts (Landman et al. 2012, Yuan et al.  
392 2014). The recent improvements of dynamical model SST forecasts (Wang et al.  
393 2009), which lead to improved guidance on the future conditions of ENSO and the  
394 SOID, provide optimism for seasonal prediction of Southern Africa precipitation (Yuan  
395 et al. 2014), where SST play a critical role in the regional climate. Here, we have  
396 identified a mechanism by which the SOID can disrupt and modulate the important  
397 ENSO-related atmosphere and precipitation response over Southern Africa.  
398 Therefore, the information presented here can be used alongside improved statistical  
399 and dynamical forecasts to make more informed Southern Africa precipitation  
400 forecasts during the November-March rainy season.

401

402 *Acknowledgements*

403           The authors thank Dave Allured for completing the ECHAM5 simulations and  
404   Tao Zhang for completing the GFSv2 simulations. The authors are grateful for  
405   support from the Famine Early Warning Systems Network (FEWS NET).  
406

407 **References**

- 408 Adler, R. F., et al. (2003), The Version-2 Global Precipitation Climatology Project  
409 (GPCP) Monthly Precipitation Analysis (1979–Present), *Journal of*  
410 *Hydrometeorology*, *4*(6), 1147-1167, doi:10.1175/1525-  
411 7541(2003)004<1147:TVGPCP>2.0.CO;2.
- 412 Behera, S. K., J.-J. Luo, S. Masson, P. Delecluse, S. Gualdi, A. Navarra, and T. Yamagata  
413 (2005), Paramount Impact of the Indian Ocean Dipole on the East African Short  
414 Rains: A CGCM Study, *Journal of Climate*, *18*(21), 4514-4530,  
415 doi:10.1175/JCLI3541.1.
- 416 Behera, S. K., P. S. Salvekar, and T. Yamagata (2000), Simulation of Interannual SST  
417 Variability in the Tropical Indian Ocean, *Journal of Climate*, *13*(19), 3487-3499,  
418 doi:10.1175/1520-0442(2000)013<3487:SOISVI>2.0.CO;2.
- 419 Behera, S. K., and T. Yamagata (2001), Subtropical SST dipole events in the southern  
420 Indian Ocean, *Geophysical Research Letters*, *28*(2), 327-330,  
421 doi:10.1029/2000GL011451.

422 Chambers, D. P., B. D. Tapley, and R. H. Stewart (1999), Anomalous warming in the  
423 Indian Ocean coincident with El Niño, *Journal of Geophysical Research: Oceans*,  
424 *104*(C2), 3035-3047, doi:10.1029/1998JC900085.

425 Gates, W. L. (1992), AMIP: The Atmospheric Model Intercomparison Project, *Bulletin*  
426 *of the American Meteorological Society*, *73*(12), 1962-1970, doi:10.1175/1520-  
427 0477(1992)073<1962:ATAMIP>2.0.CO;2.

428 Goddard, L., and N. E. Graham (1999), Importance of the Indian Ocean for simulating  
429 rainfall anomalies over eastern and southern Africa, *Journal of Geophysical*  
430 *Research: Atmospheres*, *104*(D16), 19099-19116, doi:10.1029/1999JD900326.

431 Hastenrath, S., L. Greischar, and J. van Heerden (1995), Prediction of the Summer  
432 Rainfall over South Africa, *Journal of Climate*, *8*(6), 1511-1518, doi:10.1175/1520-  
433 0442(1995)008<1511:POTSRO>2.0.CO;2.

434 Hoell, A., C. Funk, T. Magadzire, J. Zinke, and G. Husak (2015), El Niño–Southern  
435 Oscillation diversity and Southern Africa teleconnections during Austral Summer,  
436 *Clim Dyn*, *45*(5-6), 1583-1599, doi:10.1007/s00382-014-2414-z.

437 Huffman, G. J., R. F. Adler, D. T. Bolvin, and G. Gu (2009), Improving the global  
438 precipitation record: GPCP Version 2.1, *Geophysical Research Letters*, 36(17), n/a-  
439 n/a, doi:10.1029/2009GL040000.

440 Hurrell, J. W., J. J. Hack, D. Shea, J. M. Caron, and J. Rosinski (2008), A New Sea  
441 Surface Temperature and Sea Ice Boundary Dataset for the Community  
442 Atmosphere Model, *Journal of Climate*, 21(19), 5145-5153,  
443 doi:10.1175/2008JCLI2292.1.

444 Jury, M. R., C. Mc Queen, and K. Levey (1994), SOI and QBO signals in the African  
445 region, *Theor Appl Climatol*, 50(1-2), 103-115, doi:10.1007/BF00864907.

446 Landman, W. A., D. DeWitt, D.-E. Lee, A. Beraki, and D. Lötter (2011), Seasonal Rainfall  
447 Prediction Skill over South Africa: One- versus Two-Tiered Forecasting Systems,  
448 *Weather and Forecasting*, 27(2), 489-501, doi:10.1175/WAF-D-11-00078.1.

449 Landman, W. A., and L. Goddard (2005), Predicting southern African summer rainfall  
450 using a combination of MOS and perfect prognosis, *Geophysical Research*  
451 *Letters*, 32(15), n/a-n/a, doi:10.1029/2005GL022910.

452 Lindesay, J. A. (1988), South African rainfall, the Southern Oscillation and a Southern  
453 Hemisphere semi-annual cycle, *Journal of Climatology*, 8(1), 17-30,  
454 doi:10.1002/joc.3370080103.

455 Manatsa, D., C. H. Matarira, and G. Mukwada (2011), Relative impacts of ENSO and  
456 Indian Ocean dipole/zonal mode on east SADC rainfall, *International Journal of*  
457 *Climatology*, 31(4), 558-577, doi:10.1002/joc.2086.

458 Manatsa, D., C. J. C. Reason, and G. Mukwada (2012), On the decoupling of the  
459 IODZM from southern Africa Summer rainfall variability, *International Journal of*  
460 *Climatology*, 32(5), 727-746, doi:10.1002/joc.2306.

461 Misra, V. (2003), The Influence of Pacific SST Variability on the Precipitation over  
462 Southern Africa, *Journal of Climate*, 16(14), 2408-2418, doi:10.1175/2785.1.

463 Nicholson, S., and D. Entekhabi (1986), The quasi-periodic behavior of rainfall  
464 variability in Africa and its relationship to the southern oscillation, *Arch. Met.*  
465 *Geoph. Biocl. A.*, 34(3-4), 311-348, doi:10.1007/BF02257765.

466 Nicholson, S. E. (1997), AN ANALYSIS OF THE ENSO SIGNAL IN THE TROPICAL  
467 ATLANTIC AND WESTERN INDIAN OCEANS, *International Journal of Climatology*,



468 17(4), 345-375, doi:10.1002/(SICI)1097-0088(19970330)17:4<345::AID-  
469 JOC127>3.0.CO;2-3.

470 Nicholson, S. E., and J. Kim (1997), THE RELATIONSHIP OF THE EL NIÑO–SOUTHERN  
471 OSCILLATION TO AFRICAN RAINFALL, *International Journal of Climatology*, 17(2),  
472 117-135, doi:10.1002/(SICI)1097-0088(199702)17:2<117::AID-JOC84>3.0.CO;2-O.

473 Ratnam, J. V., S. K. Behera, Y. Masumoto, and T. Yamagata (2014), Remote Effects of  
474 El Niño and Modoki Events on the Austral Summer Precipitation of Southern  
475 Africa, *Journal of Climate*, 27(10), 3802-3815, doi:10.1175/JCLI-D-13-00431.1.

476 Reason, C. J. C. (2001), Subtropical Indian Ocean SST dipole events and southern  
477 African rainfall, *Geophysical Research Letters*, 28(11), 2225-2227,  
478 doi:10.1029/2000GL012735.

479 Reason, C. J. C., R. J. Allan, J. A. Lindesay, and T. J. Ansell (2000), ENSO and climatic  
480 signals across the Indian Ocean Basin in the global context: part I, interannual  
481 composite patterns, *International Journal of Climatology*, 20(11), 1285-1327,  
482 doi:10.1002/1097-0088(200009)20:11<1285::AID-JOC536>3.0.CO;2-R.

483 Reason, C. J. C., and D. Jagadheesha (2005), A model investigation of recent ENSO  
484 impacts over southern Africa, *Meteorol. Atmos. Phys.*, *89*(1-4), 181-205,  
485 doi:10.1007/s00703-005-0128-9.

486 Rocha, A., and I. A. N. Simmonds (1997), INTERANNUAL VARIABILITY OF SOUTH-  
487 EASTERN AFRICAN SUMMER RAINFALL. PART 1: RELATIONSHIPS WITH AIR-SEA  
488 INTERACTION PROCESSES, *International Journal of Climatology*, *17*(3), 235-265,  
489 doi:10.1002/(SICI)1097-0088(19970315)17:3<235::AID-JOC123>3.0.CO;2-N.

490 Roeckner, E., R. Brokopf, M. Esch, M. Giorgetta, S. Hagemann, L. Kornblueh, E.  
491 Manzini, U. Schlese, and U. Schulzweida (2006), Sensitivity of Simulated Climate  
492 to Horizontal and Vertical Resolution in the ECHAM5 Atmosphere Model, *Journal*  
493 *of Climate*, *19*(16), 3771-3791, doi:10.1175/JCLI3824.1.

494 Saha, S., et al. (2013), The NCEP Climate Forecast System Version 2, *Journal of*  
495 *Climate*, *27*(6), 2185-2208, doi:10.1175/JCLI-D-12-00823.1.

496 Saji, N. H., B. N. Goswami, P. N. Vinayachandran, and T. Yamagata (1999), A dipole  
497 mode in the tropical Indian Ocean, *Nature*, *401*(6751), 360-363.

498 Wang, B., et al. (2009), Advance and prospectus of seasonal prediction: assessment of  
499 the APCC/CliPAS 14-model ensemble retrospective seasonal prediction (1980–  
500 2004), *Clim Dyn*, 33(1), 93-117, doi:10.1007/s00382-008-0460-0.

501 Washington, R., and A. Preston (2006), Extreme wet years over southern Africa: Role  
502 of Indian Ocean sea surface temperatures, *Journal of Geophysical Research:*  
503 *Atmospheres*, 111(D15), n/a-n/a, doi:10.1029/2005JD006724.

504 Webster, P. J., A. M. Moore, J. P. Loschnigg, and R. R. Leben (1999), Coupled ocean-  
505 atmosphere dynamics in the Indian Ocean during 1997-98, *Nature*, 401(6751),  
506 356-360,  
507 doi:[http://www.nature.com/nature/journal/v401/n6751/suppinfo/401356a0\\_S1.ht](http://www.nature.com/nature/journal/v401/n6751/suppinfo/401356a0_S1.html)  
508 [ml](http://www.nature.com/nature/journal/v401/n6751/suppinfo/401356a0_S1.html).

509 Wyrtki, K. (1975), El Niño—The Dynamic Response of the Equatorial Pacific Ocean to  
510 Atmospheric Forcing, *Journal of Physical Oceanography*, 5(4), 572-584,  
511 doi:10.1175/1520-0485(1975)005<0572:ENTDRO>2.0.CO;2.

512 Yuan, C., T. Tozuka, W. Landman, and T. Yamagata (2014), Dynamical seasonal  
513 prediction of Southern African summer precipitation, *Clim Dyn*, 42(11-12), 3357-  
514 3374, doi:10.1007/s00382-013-1923-5.

515

516

517 **List of Figures**

518 Figure 1: Correlation of November-March 1979-2014 SST anomaly and (a) the  
519 Niño3.4 index anomaly, (b) the IOD index anomaly and (c) the SIOD index  
520 anomaly. Shading indicates correlations significant at  $p < 0.10$ . The Niño3.4  
521 index is defined as areal average SST over 5°S-5°N; 170°W-120°W shown as the  
522 green outline in panel (a). The IOD index is defined as areal average SST over  
523 10°S-0°N; 90°E-110°E subtracted from areal average SST over 10°S-10°N; 50°E-  
524 70°E, both of which are shown as green outlines on panel (b). The SIOD index is  
525 defined as areal average SST over 28°S-18°N; 90°E-100°E subtracted from areal  
526 average SST over 37°S-27°S; 55°E-65°E, both of which are shown as green  
527 outlines on panel (c).....39

528 Figure 2: November-March 1979-2014 correlation of observed Southern Africa  
529 precipitation anomaly with (a) observed spatial precipitation anomaly and (b)  
530 observed SST anomaly. Shading indicates correlations significant at  $p < 0.10$ .....41

531 Figure 3: November-March (top) SST anomaly in units of K and (bottom)  
532 precipitation anomaly in units of mm d<sup>-1</sup> during El Niño and La Niña events in  
533 which the Niño3.4 index anomaly and SIOD index anomaly have the same and

534 opposing signs. El Niño (La Niña) events are defined when the November-

535 March Niño3.4 index anomaly exceeds (falls below) 0.5K (-0.5K).....42

536 Figure 4: (a) The leading pattern of global SST anomaly in units of K calculated using

537 a covariance-based empirical orthogonal function (EOF1) and (b) associated

538 principal component for 1978-2014.....43

539 Figure 5: (top) November-March 1979-2014 average rainfall (cm) and (bottom)

540 monthly average 1979-2014 rainfall (cm) in (left column) GPCP, (center column)

541 30 ECHAM5 AMIP simulations and (right column) 50 GFS version 2 AMIP

542 simulations. ....44

543 Figure 6: Simulated November-March 1979-2014 standardized Southern Africa

544 precipitation anomaly forced by (a) global SST and (b) EOF1 of SST. Green dots

545 indicate individual simulated ensembles, the red line shows the simulated

546 ensemble average and the blue line shows observed precipitation.....45

547 Figure 7: November-March 1979-2014 correlation of observed SST anomaly and

548 simulated precipitation forced by (a) global SST and (b) EOF1 of SST. Shading

549 denotes correlations significant at  $p < 0.10$ .....46

550 Figure 8: (top row) Correlation of simulated Southern Africa standardized  
 551 precipitation anomaly forced by global SST with global SST. (bottom row)  
 552 Scatter diagrams of observed Niño3.4 anomaly and simulated Southern Africa  
 553 standardized precipitation anomaly forced by global SST (green dots) with the  
 554 least squares regression line shown in red. Results are for November-March  
 555 1979-2014 and are shown (left column) in aggregate, (center column) when the  
 556 Niño3.4 and SIOD indices have the opposite sign and (right column) when the  
 557 Niño3.4 and SIOD indices have the same sign. Shading denotes correlations  
 558 significant at  $p < 0.10$ . .....47

559 Figure 9: Correlation of Niño3.4 anomaly and simulated global SST-forced (top)  
 560 standardized precipitation anomaly and (bottom) 700 hPa wind anomaly (vector)  
 561 and 400 hPa vertical velocity anomaly (shading) for November-March 1979-2014  
 562 (left column) in aggregate, (center column) when the Niño3.4 and SIOD indices  
 563 have the opposite sign and (right column) when the Niño3.4 and SIOD indices  
 564 have the same sign. Shading denotes correlations significant at  $p < 0.10$ . .....48

565 Figure 10: (top row) Correlation of simulated Southern Africa standardized  
 566 precipitation anomaly forced by EOF1 with global SST. (bottom row) Scatter

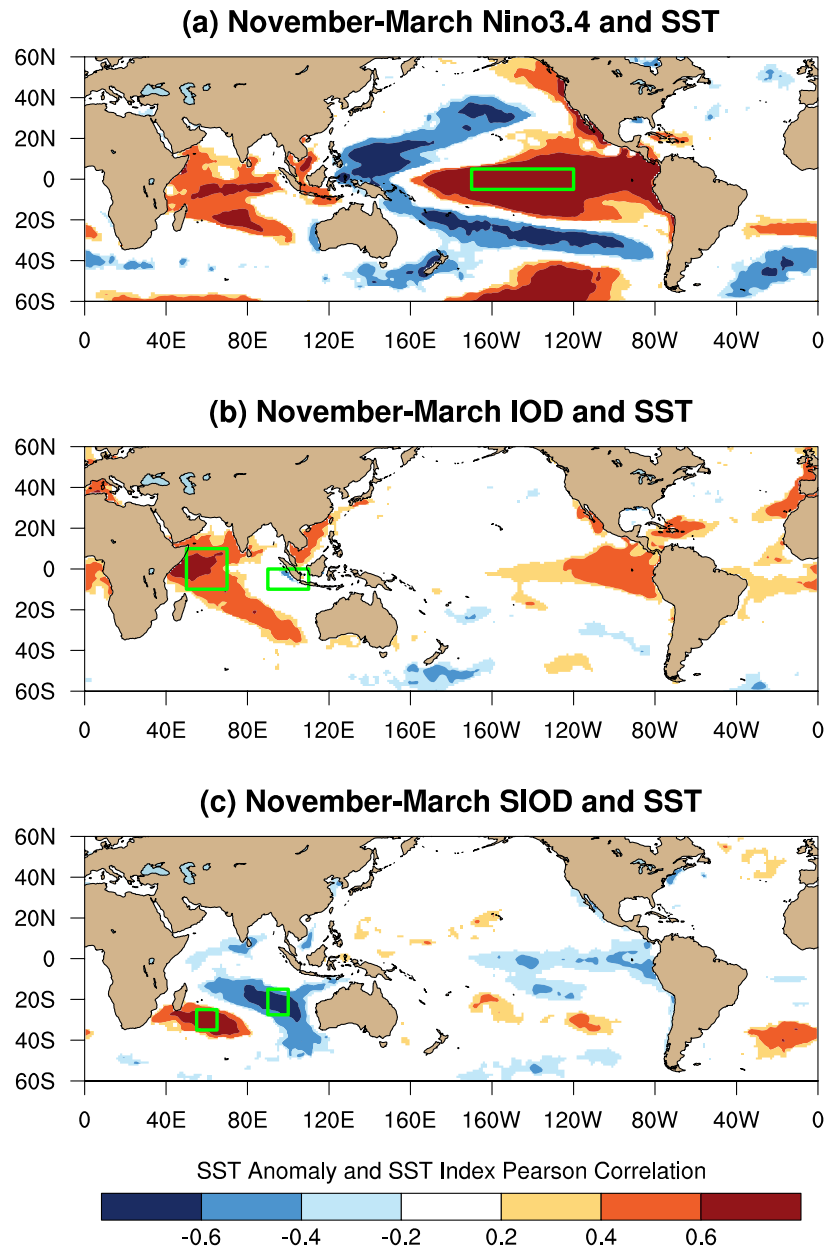
567 diagrams of observed Niño3.4 anomaly and simulated Southern Africa  
568 standardized precipitation anomaly forced by EOF1 (green dots) with the least  
569 squares regression line shown in red. Results are for November-March 1979-  
570 2014 and are shown (left column) in aggregate, (center column) when the  
571 Niño3.4 and SIOD indices have the opposite sign and (right column) when the  
572 Niño3.4 and SIOD indices have the same sign. Shading denotes correlations  
573 significant at  $p < 0.10$ . .....49

574 Figure 11: Correlation of Niño3.4 anomaly and simulated EOF1-forced (top)  
575 standardized precipitation anomaly and (bottom) 700 hPa wind anomaly (vector)  
576 and 400 hPa vertical velocity anomaly (shading) for November-March 1979-2014  
577 (left column) in aggregate, (center column) when the Niño3.4 and SIOD indices  
578 have the opposite sign and (right column) when the Niño3.4 and SIOD indices  
579 have the same sign. Shading denotes correlations significant at  $p < 0.10$ . .....50

580

581



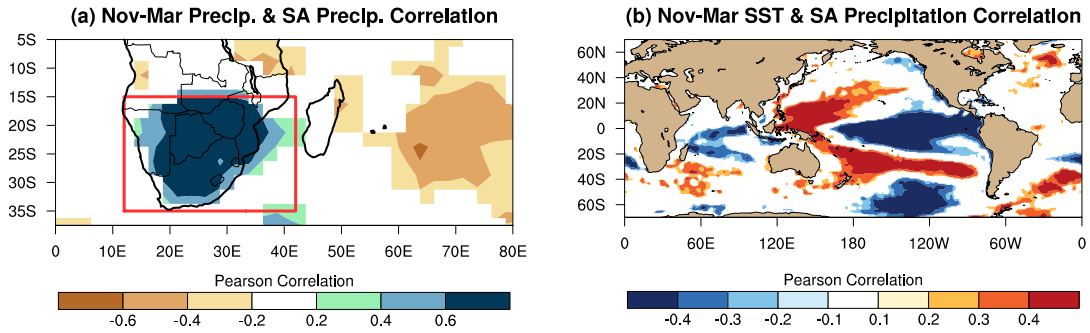


583

584 Figure 1: Correlation of November-March 1979-2014 SST anomaly and (a) the  
 585 Niño3.4 index anomaly, (b) the IOD index anomaly and (c) the SIOD index anomaly.  
 586 Shading indicates correlations significant at  $p < 0.10$ . The Niño3.4 index is defined as  
 587 areal average SST over 5°S-5°N; 170°W-120°W shown as the green outline in panel  
 588 (a). The IOD index is defined as areal average SST over 10°S-0°N; 90°E-110°E  
 589 subtracted from areal average SST over 10°S-10°N; 50°E-70°E, both of which are  
 590 shown as green outlines on panel (b). The SIOD index is defined as areal average SST

591 over 28°S-18°N; 90°E-100°E subtracted from areal average SST over 37°S-27°S; 55°E-  
592 65°E, both of which are shown as green outlines on panel (c).

593



594

595

Figure 2: November-March 1979-2014 correlation of observed Southern Africa

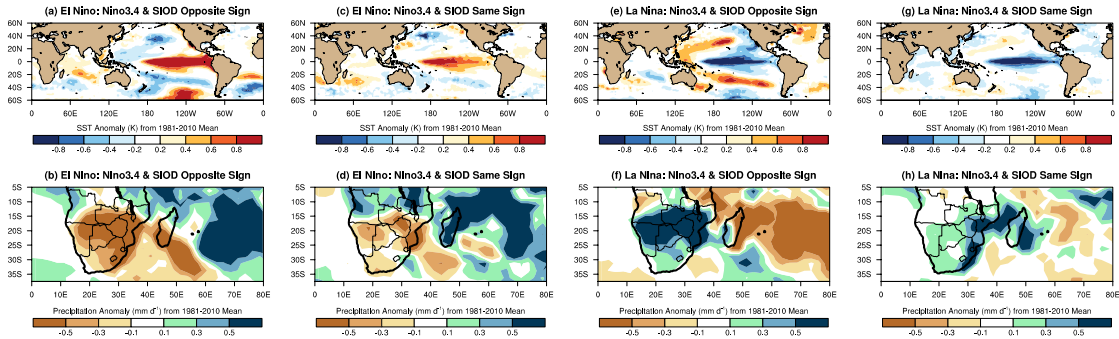
596

precipitation anomaly with (a) observed spatial precipitation anomaly and (b)

597

observed SST anomaly. Shading indicates correlations significant at  $p < 0.10$ .

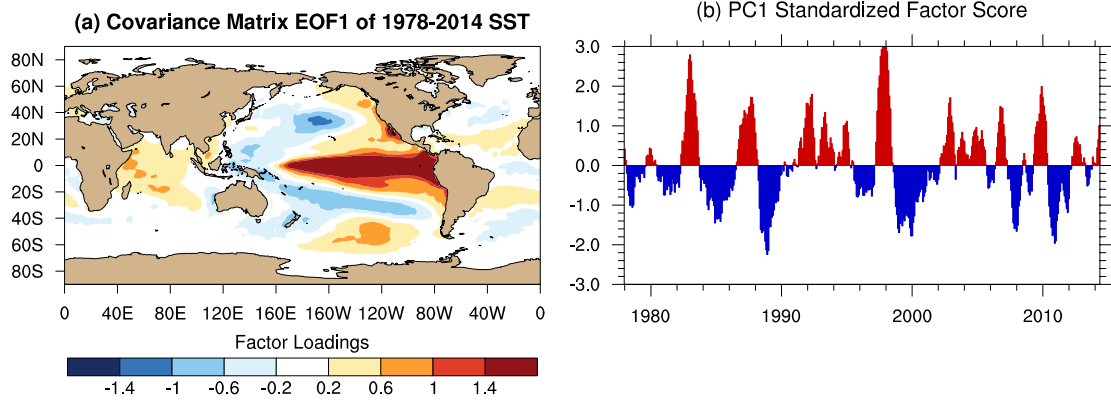
598



599

600 Figure 3: November-March (top) SST anomaly in units of K and (bottom)  
 601 precipitation anomaly in units of  $\text{mm d}^{-1}$  during El Niño and La Niña events in which  
 602 the Niño3.4 index anomaly and SIOD index anomaly have the same and opposing  
 603 signs. El Niño (La Niña) events are defined when the November-March Niño3.4  
 604 index anomaly exceeds (falls below)  $0.5\text{K}$  ( $-0.5\text{K}$ ).

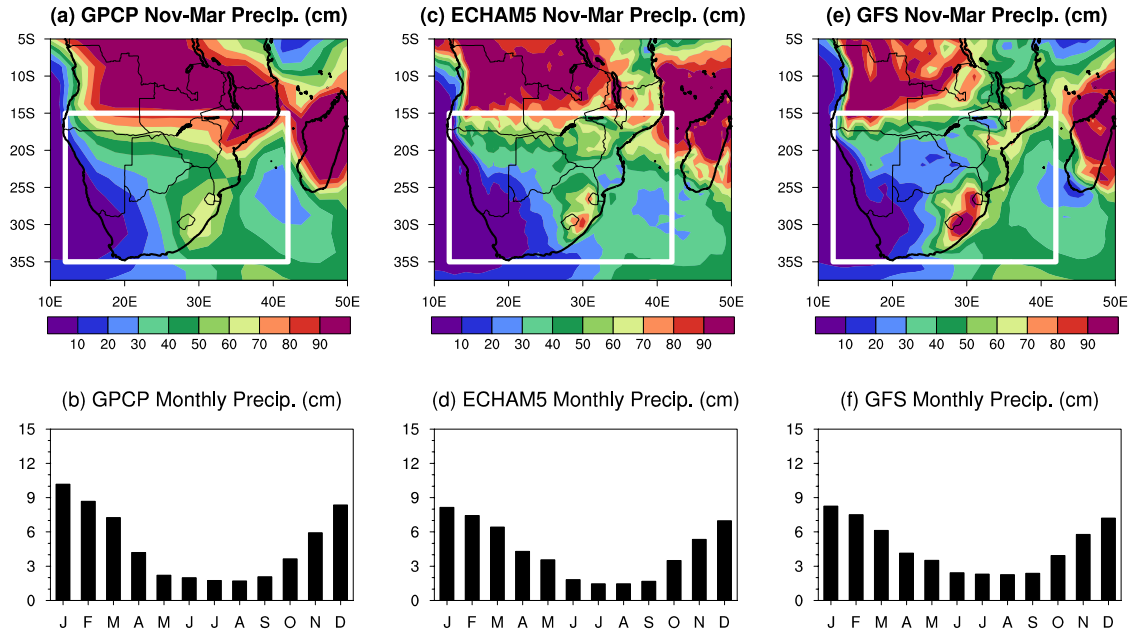
605



606

607 Figure 4: (a) The leading pattern of global SST anomaly in units of K calculated using  
 608 a covariance-based empirical orthogonal function (EOF1) and (b) associated principal  
 609 component for 1978-2014.

610



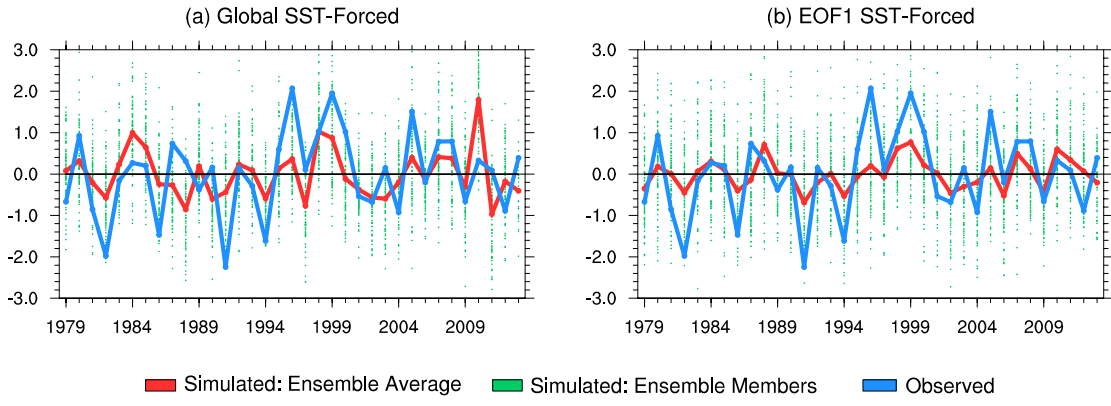
611

612 Figure 5: (top) November-March 1979-2014 average rainfall (cm) and (bottom)

613 monthly average 1979-2014 rainfall (cm) in (left column) GPCP, (center column) 30

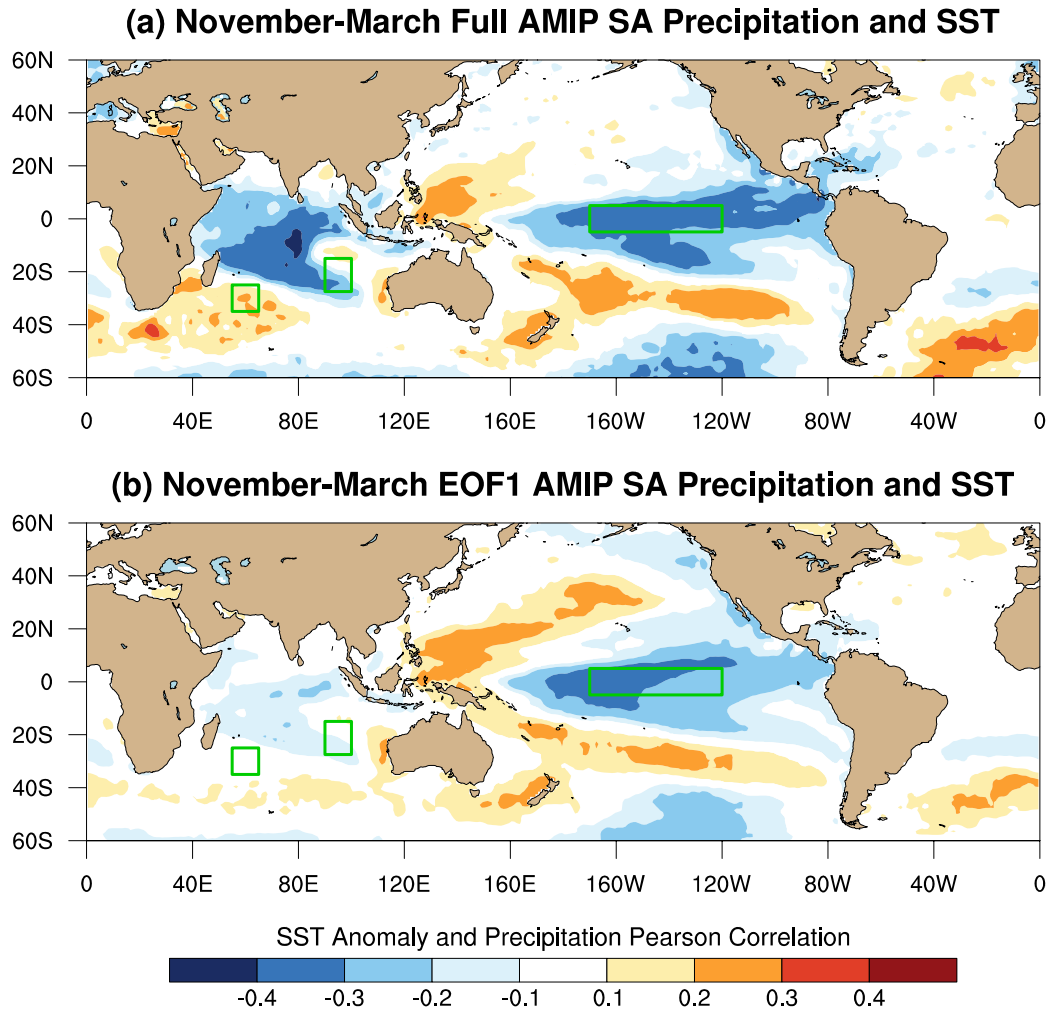
614 ECHAM5 AMIP simulations and (right column) 50 GFS version 2 AMIP simulations.

615



616  
 617  
 618  
 619  
 620  
 621

Figure 6: Simulated November-March 1979-2014 standardized Southern Africa precipitation anomaly forced by (a) global SST and (b) EOF1 of SST. Green dots indicate individual simulated ensembles, the red line shows the simulated ensemble average and the blue line shows observed precipitation.

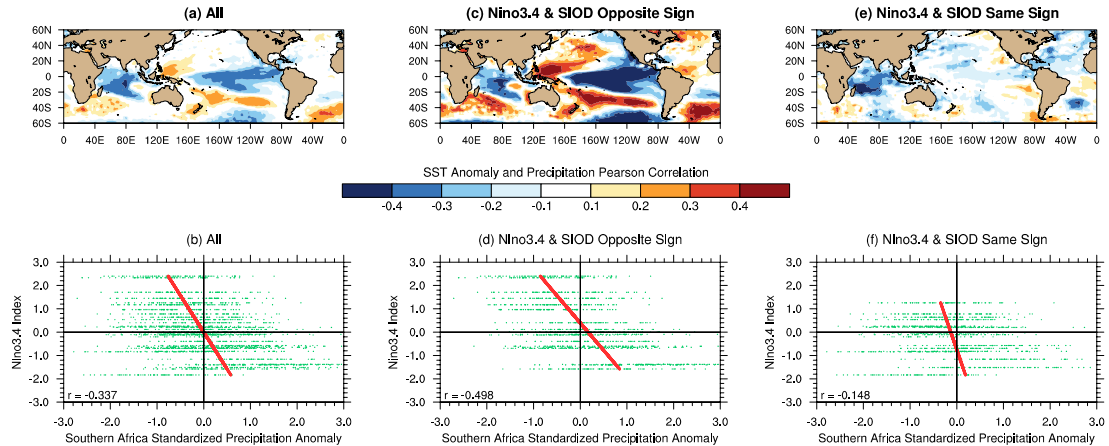


622

623 Figure 7: November-March 1979-2014 correlation of observed SST anomaly and  
 624 simulated precipitation forced by (a) global SST and (b) EOF1 of SST. Shading  
 625 denotes correlations significant at  $p < 0.10$ .

626

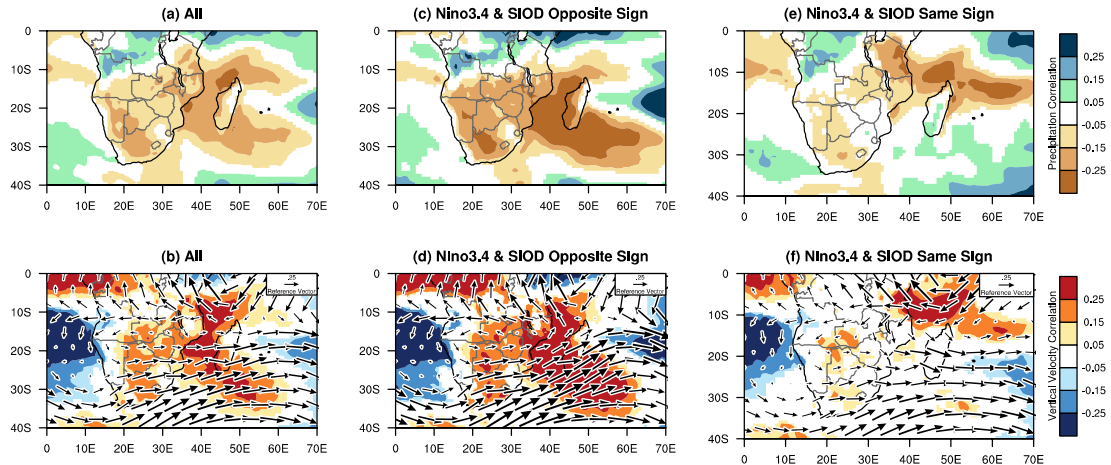




627

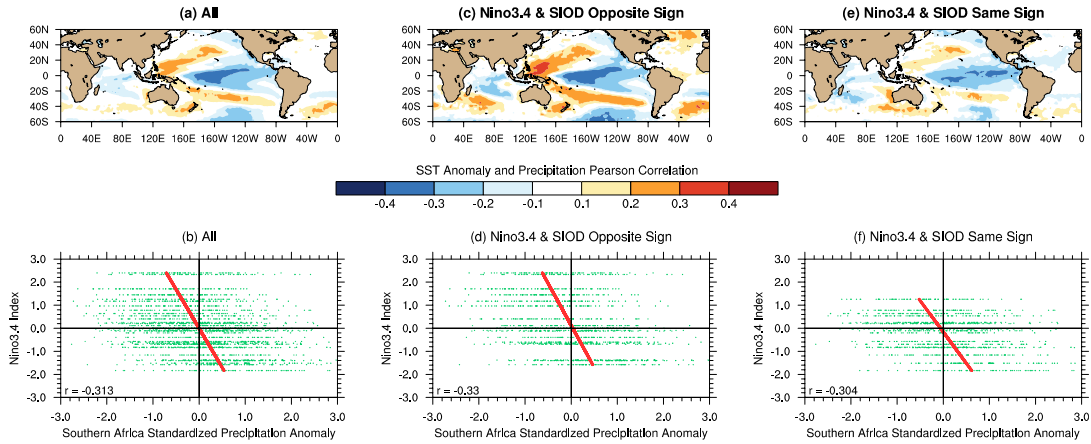
628 Figure 8: (top row) Correlation of simulated Southern Africa standardized  
 629 precipitation anomaly forced by global SST with global SST. (bottom row) Scatter  
 630 diagrams of observed Niño3.4 anomaly and simulated Southern Africa standardized  
 631 precipitation anomaly forced by global SST (green dots) with the least squares  
 632 regression line shown in red. Results are for November-March 1979-2014 and are  
 633 shown (left column) in aggregate, (center column) when the Niño3.4 and SIOD  
 634 indices have the opposite sign and (right column) when the Niño3.4 and SIOD  
 635 indices have the same sign. Shading denotes correlations significant at  $p < 0.10$ .

636



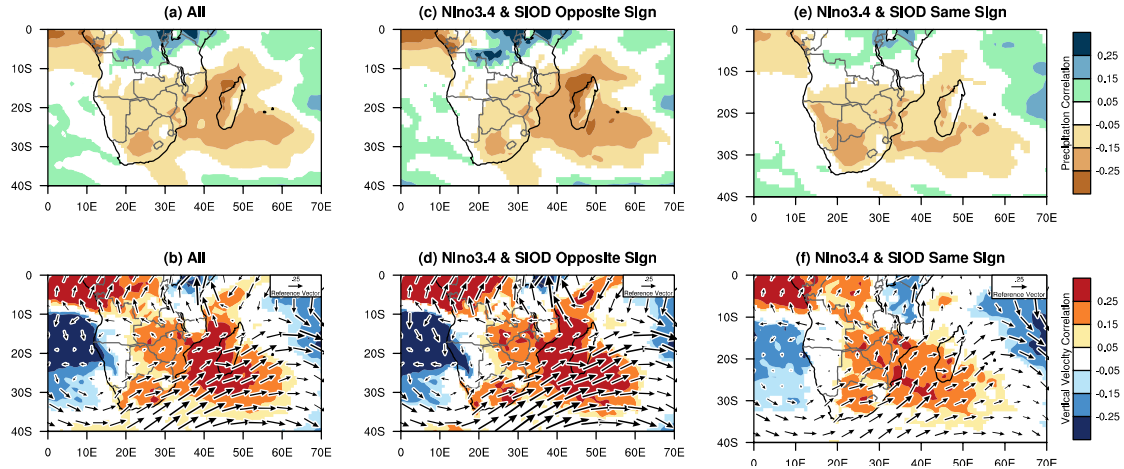
637  
 638 Figure 9: Correlation of Niño3.4 anomaly and simulated global SST-forced (top)  
 639 standardized precipitation anomaly and (bottom) 700 hPa wind anomaly (vector) and  
 640 400 hPa vertical velocity anomaly (shading) for November-March 1979-2014 (left  
 641 column) in aggregate, (center column) when the Niño3.4 and SIOD indices have the  
 642 opposite sign and (right column) when the Niño3.4 and SIOD indices have the same  
 643 sign. Shading denotes correlations significant at  $p < 0.10$ .

644



645  
 646 Figure 10: (top row) Correlation of simulated Southern Africa standardized  
 647 precipitation anomaly forced by EOF1 with global SST. (bottom row) Scatter  
 648 diagrams of observed Niño3.4 anomaly and simulated Southern Africa standardized  
 649 precipitation anomaly forced by EOF1 (green dots) with the least squares regression  
 650 line shown in red. Results are for November-March 1979-2014 and are shown (left  
 651 column) in aggregate, (center column) when the Niño3.4 and SIOD indices have the  
 652 opposite sign and (right column) when the Niño3.4 and SIOD indices have the same  
 653 sign. Shading denotes correlations significant at  $p < 0.10$ .

654



655

656 Figure 11: Correlation of Niño3.4 anomaly and simulated EOF1-forced (top)  
 657 standardized precipitation anomaly and (bottom) 700 hPa wind anomaly (vector) and  
 658 400 hPa vertical velocity anomaly (shading) for November-March 1979-2014 (left  
 659 column) in aggregate, (center column) when the Niño3.4 and SIOD indices have the  
 660 opposite sign and (right column) when the Niño3.4 and SIOD indices have the same  
 661 sign. Shading denotes correlations significant at  $p < 0.10$ .

662